



## Partitioning of coal contaminants in the components of liquid tin anode solid oxide fuel cells

Benjamin C. Nielsen<sup>a,b,\*</sup>, Kirk Gerdes<sup>c</sup>, William O'Connor<sup>a</sup>, Xueyan Song<sup>d</sup>, Harry Abernathy<sup>c</sup>

<sup>a</sup>National Energy Technology Laboratory, 1450 Queen Ave. SW, Albany, OR 97321, United States

<sup>b</sup>URS Corporation (NETL site contractor), United States

<sup>c</sup>National Energy Technology Laboratory, 3610 Collins Ferry Rd., Morgantown, WV 26507, United States

<sup>d</sup>West Virginia University, Engineering Sciences Bldg, Evansdale Dr., Morgantown, WV 26506, United States

### ARTICLE INFO

#### Article history:

Received 21 December 2011

Received in revised form

15 March 2012

Accepted 17 March 2012

Available online 7 April 2012

#### Keywords:

Solid oxide fuel cell

Liquid metal anode

Tin

Direct carbon

Coal contaminants

### ABSTRACT

Direct carbon fuel cells (DCFCs) electrochemically convert fossil fuels to electricity, resulting in higher efficiency and less pollution than traditional direct combustion technologies. This work focuses on direct use of coal in a liquid tin anode solid oxide fuel cell (LTA SOFC) where a layer of molten tin functions as the anode. In such a direct solid fueling scheme, a major technical concern is the ultimate disposition of trace materials naturally present in the coal. Trace contaminants introduced with the coal must be located in the functional portions of the LTA SOFC to ensure that any deleterious reactions are known and ultimately mitigated. This research effort determines the thermochemical contaminant partitioning between the tin anode, slag, or electrolyte material and examines the critical interfaces within the system. Contaminant partitioning was examined by TEM, SEM/EDS, and ICP–OES/MS. Sulfur is known to poison yttria-stabilized zirconia (YSZ) and appears to form a tin sulfide phase that is dispersed in the liquid tin during operation. Results show that tin oxide formed on and near the YSZ electrolyte, and could potentially degrade charge transfer. The slag was found to consist of the expected metal oxides, however, tin and tin oxide were intermixed with the slag component, indicating a probable need for a tin recovery process that will potentially increase the complexity of an LTA SOFC system.

© 2012 Elsevier B.V. All rights reserved.

### 1. Introduction

Fuel cell technology offers a higher efficiency, lower pollution alternative to combustion of fossil fuels for electricity generation. The use of pure hydrogen fuel in a fuel cell produces only water, and one method of obtaining hydrogen is from steam reforming of hydrocarbons. Reacting hydrocarbons and steam to produce hydrogen presents its own set of difficulties, including carryover of trace contaminants to the produced gas stream. Solid oxide fuel cells (SOFCs) are somewhat more robust than other fuel cell types and can tolerate some amount of compositional variation in fuels [1]. Coal is one such domestically abundant fuel source, and coal-derived stationary power generation is projected to dominate the U.S. market through 2035 [2]. Technology is being explored by the National Energy Technology Laboratory (NETL) to utilize coal for stationary power generation with higher efficiency while

decreasing its environmental impact. The U.S. Department of Energy's (DOE) Solid State Energy Conversion Alliance (SECA) program is a collaboration between the DOE, universities, and private industry to advance SOFC technology for use in utility-scale power plants that is competitive with conventional power cycles. A conceptual Integrated Gasification Fuel Cell (IGFC) power plant would gasify coal and supply syngas to a SOFC in a process with efficiency exceeding 56% [3]. Coupled with CO<sub>2</sub> sequestration, the IGFC cuts CO<sub>2</sub> emissions and improves efficiency relative to traditional combustion processes.

An alternative to the IGFC that is potentially attractive for power generation applications smaller than utility scale (distributed generation) is to provide coal directly to the fuel cell, thereby potentially increasing system efficiency and decreasing the system cost by eliminating the gasifier. Various types of direct carbon fuel cells (DCFCs) have been reported recently [4,5] including molten carbonate fuel cells (MCFCs) and SOFCs. Reported designs use carbon particles produced from the pyrolysis of hydrocarbons including coal [6,7] and reaction products from *in situ* dry gasification of coal [8]. Common SOFC anode materials consist of Ni–yttria stabilized zirconia (YSZ) cermets, and when using

\* Corresponding author. National Energy Technology Laboratory, 1450 Queen Ave. SW, Albany, OR 97321, United States. Tel.: +1 541 918 8073; fax: +1 541 918 4493.

E-mail address: [Benjamin.Nielsen@contr.netl.doe.gov](mailto:Benjamin.Nielsen@contr.netl.doe.gov) (B.C. Nielsen).

hydrocarbons directly in a SOFC these materials are susceptible to carbon formation (coking) [9,10] and sulfur attack [11,12]. Therefore, SOFCs have been developed using alternative anode materials that are more tolerant to coking and contaminants [10] including Cu–ceria [9,13,14], which have been successfully run on various liquid and gaseous hydrocarbon fuels.

The liquid metal anode solid oxide fuel cell (LMA SOFC) is a novel direct coal fuel cell concept being investigated by NETL and collaborators [15], and may be another alternative anode formulation that is tolerant to contaminant attack. CellTech Power has actively developed this fuel cell over more than a decade and has received several patents [16,17]. A schematic of the basic operational principles is shown in Fig. 1. The usual Ni cermet anode in a standard SOFC is replaced with a layer of molten metal. Tin has been explored as the liquid metal, as in the focus of this work, but other metals have also been reported such as Bi and Pb [18,19] and some alloys. During operation, oxygen is ionized at the cathode, which is typically composed of lanthanum strontium manganite (LSM). The oxygen anion traverses the YSZ electrolyte and diffuses into the liquid metal layer where it ultimately oxidizes the fuel (coal in this case).

The LMA SOFC design and continued development efforts will be influenced by interactions of coal with the fuel cell components. In particular, contaminant partitioning first must be examined thermochemically to determine the intrinsic chemical drivers present in the initial thermodynamic state. Coal is a complex solid material containing ash-forming inorganics, trace heavy metals, and Sulfur, all of which may interfere with the fuel cell to negatively impact performance [20]. During the coal chemical reaction in a LMA SOFC it is desirable for the non-combustible and non-volatile components to remain with the unreducible portion of the coal (slag), which can subsequently be removed in a skimming or filtration process. However, some contaminants may exhibit sufficient solubility in the molten tin to have a detrimental effect on cell operation by affecting the physical properties or chemically attacking active system components. For example, numerous studies demonstrate that YSZ is especially susceptible to attack from even small concentrations of sulfur, down to sub-ppm [11,12,21–23]. These studies all look at Ni-based anode SOFCs as opposed to LMAs, however, the results focus specifically on sulfur poisoning of the YSZ electrolyte material so they are applicable to LMA SOFCs since the electrolyte is identical in all cases. The key technical task of this work was to evaluate potentially negative contaminant interactions, and especially to examine contaminant partitioning between the coal, slag, and cell components. Partitioning of common coal contaminants including As, Cr, P, S, and V

was examined between the primary cell zones: the YSZ electrolyte material, the tin, and the slag derived from the oxides and coal ash component. Representative U.S. eastern (Pitt Seam) and western (Wyodak) coals were used for the study.

## 2. Experimental procedure

Thermochemical experiments were conducted to reduce a small amount of tin oxide, mixed with tin metal, using coal in yttria-stabilized zirconia (YSZ) crucibles. Half liter volume, straight-sided sintered YSZ crucibles (5.2 at%  $\text{Y}_2\text{O}_3$ , 0.3 at%  $\text{CaO}$ , 0.3 at%  $\text{SiO}_2$ , 0.3 at%  $\text{Al}_2\text{O}_3$ ) obtained from Zircoa were used. Two types of coal obtained from the Penn State University Coal Bank were used, an eastern Pittsburgh Seam Coal (DECS-34) and a western Wyodak coal (DECS-26), both chosen for their representative composition and ubiquitous consumption in domestic energy production. The coals were ground to  $<75\ \mu\text{m}$  and dried at  $100\ ^\circ\text{C}$ . High purity tin oxide powder (99.9%  $\text{SnO}_2$ ,  $<75\ \mu\text{m}$ ) was obtained from Universal Photonics. High purity tin shot (99.99% Sn,  $<595\ \mu\text{m}$ ) was obtained from Atlantic Equipment Engineers. It is recognized that the setup for these exposure tests is not necessarily identical to the conditions seen in an electrochemically active cell that is generating power. The mixtures were so composed and thermally treated to determine the contaminant partitioning due to purely thermochemical drivers, and no examination of the impact of electrochemical operation is examined in this work.

A total of 6 samples were prepared, three from each coal. The tin, tin oxide, and coals were weighed out using a Mettler Toledo digital balance accurate to 0.01 g and blended together by hand using a micro spatula. First, the tin oxide and coal powders were mixed together, and then the tin shot was added and thoroughly mixed. The mixture containing 1250 g of tin shot and 125 g of tin oxide was placed in each crucible with to establish a tin metal to tin oxide ratio of 10:1. The added coal mass was calculated on the basis of the fixed carbon to tin oxide stoichiometry. Fixed carbon is the carbon that remains in the coal after all volatile materials are driven off. The fixed carbon in the Pitt Seam coal was 54 wt% and in the Wyodak coal was 48 wt% and neither coal was pyrolyzed prior to the tests. Reduction efficiencies of  $>90\%$  for the two coal types were determined in preliminary tests using only tin oxide and coal. The test results indicated that the highest reduction efficiencies were at 100% stoichiometry for the Pitt Seam coal and 115% for the Wyodak coal at  $1000\ ^\circ\text{C}$ . Consequently, 18.28 g of Pitt Seam coal and 23.99 g of Wyodak coal were added to each crucible for the respective test vessels. The slag-forming inorganic oxide content of each coal was determined by high-temperature ash (HTA) analysis, and results are depicted in Table 1. The total ash content was 7.57 wt% for the Wyodak coal and 7.35 wt% for the Pitt Seam coal.

Trace contaminant concentrations in the as-prepared samples were not expected to be sufficiently high enough to exceed the lower detection limit of standard inductively coupled plasma (ICP) analytical techniques. Therefore, the samples were spiked with specific contaminants of interest. Eleven trace elements of interest were identified by CellTech as both soluble in molten tin and potentially harmful to the electrolyte: As, Cr, Mn, Mo, Nb, Se, Ta, U, V, W, and Zn [20]. From this list, the elements Cr, Mo, and V were considered and were added to each crucible in an amount ten times greater than concentrations found naturally in the coals. A micro balance accurate to 0.1 mg was used to weigh out the trace contaminants, and the powders were blended with the mixture of tin oxide and coal before filling the crucible. Masses of Cr, Mo, and V metals added to the three Pitt Seam samples were 33.9 mg, 5.1 mg, and 9.6 mg, respectively. The amounts added for the Wyodak samples were 33.1 mg, 3.6 mg, and 7.8 mg, respectively.

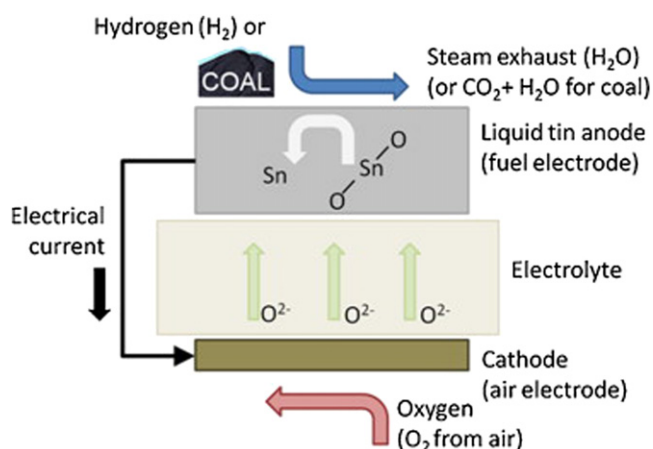


Fig. 1. Schematic of the operational principles of a liquid tin anode SOFC [15].

**Table 1**  
Slag-forming inorganic ash content (wt%) from high-temperature ash (HTA) analysis.

	Wyodak coal	Pitt Seam coal
SiO <sub>2</sub>	30.87	50.18
Al <sub>2</sub> O <sub>3</sub>	15.39	23.46
CaO	25.16	2.80
Fe <sub>2</sub> O <sub>3</sub>	6.38	14.91
MgO	4.55	0.76
TiO <sub>2</sub>	1.19	0.97
Na <sub>2</sub> O	1.22	0.53
K <sub>2</sub> O	0.33	1.85
P <sub>2</sub> O <sub>5</sub>	1.04	0.47
SO <sub>3</sub>	13.29	2.35
Total	99.40	98.25
% ash of whole dry coal	7.57	7.35

In addition to the trace metals, CaO was added to all six samples in order to establish a theoretically neutral slag (molar basicity of 1.0). The molar basicity of the slag was calculated based on the measured concentrations of basic oxides vs. acid oxides in the coal ash. The theoretical molar basicity of the unmodified Pitt Seam coal was 0.14, while that for the unmodified Wyodak coal was 0.92. A basicity less than one is considered acidic, and greater than one as basic. An addition of 0.80 g of CaO was made to the Pitt Seam samples and 0.05 g was added to the Wyodak samples to increase the molar basicity to near 1. The CaO addition to the Pittsburgh Seam coal was considered a necessary modification to produce a free-flowing slag that would aid in its physical separation from the molten tin. This separation, coupled with the partitioning of contaminants to the slag, was expected to enhance contaminant removal from the tin.

Representative YSZ (8 at% Y<sub>2</sub>O<sub>3</sub>) electrolyte pieces were also added to the crucible in specific orientations to examine the interaction of tin with materials and structures typical of the SOFC electrolyte. 250 μm thick 8YSZ disks (3.2 cm diam.) and strips (9 × 1 cm) were obtained from Fuel Cell Materials and West Virginia University. One YSZ disk was inserted horizontally in the bottom of each crucible, and a YSZ strip was placed vertically in samples P3 and W3, such that the strip extended above the top of the tin/tin oxide/coal mixture. The total contents of each of the six crucibles, labeled P1, P2, P3, W1, W2, and W3, are shown in Table 2.

The YSZ crucibles were inserted into larger alumina crucibles with the annular space packed with sand and topped with fibrous high-temperature insulation to mitigate thermal transients during insertion and removal from the furnace. The empty crucibles were purged with 99.9% argon gas at a flow rate of 200 mL per minute for ~5 min in order to provide an inert atmosphere and prevent the tin

and coal from reacting with oxygen in the air. The weighed-out mixture of tin, tin oxide, coal, spiking elements, and calcium oxide were placed in each crucible and a YSZ lid with a 1/4" hole in the middle was placed on top. A second alumina lid went over the top of the alumina crucibles. The loaded crucible was then re-purged with Ar for two minutes. The crucibles before and after loading are shown in Fig. 2a and b, respectively.

The six crucibles were inserted into a preheated Lingberg box furnace held at 1000 °C. The temperature was monitored with a k-type thermocouple in a seventh crucible that contained an identical mixture as the Pitt Seam samples, except for the spiking elements. Thermal equilibration of the samples at 1000 °C required approximately 3 h. The P1 and W1 crucibles were removed 2 h after reaching temperature, P2 and W2 were removed after 24 h, and P3 and W3 were removed after 96 h. Samples were cooled in ambient air and subsequently sectioned and polished for microscopic and SEM–EDS chemical analysis. Polishing was performed with silica, alumina, and diamond media. An FEI Inspect F50 SEM in back-scatter mode with Oxford Instruments INCA energy dispersive spectroscopy (EDS) capability was used to characterize the samples. The samples were coated with Pd, and a 20 kV excitation voltage was typically used. Quantitative analysis was performed using the EDS and Inca software. TEM samples were prepared by mechanical polishing and ion milling in a liquid-nitrogen cooled holder. Electron diffraction, diffraction contrast and high-resolution TEM imaging were performed in a JEM-2100 operated at 200 kV. Chemical analysis was carried out using EDS under TEM.

Samples for inductively coupled plasma (ICP) chemical analysis were prepared by collecting core turnings by drilling into the middle of the tin ingot in each crucible and were analyzed using ICP atomic emission spectrometer (ICP–AES) and ICP mass spectrometer (ICP–MS) methods. A full chemical analysis was also run on the as-received coal and tin oxide for comparison. The chemical analysis was conducted following standard practices. Approximately 0.3 g of the sample was weighed and placed in a beaker. Concentrated hydrochloric acid (5 mL) was added to the sample, and the beaker was placed on a magnetic stirrer to achieve complete dissolution of the sample at room temperature. The contents of the beaker were transferred to a flask and dissolved in 50 mL of de-ionized water. A procedural blank was also prepared and processed in identical conditions as the sample. A Perkin Elmer model Optima 3000 XL ICP–AES was used for all data acquisition. The trace elements that were below the detection limits of ICP–AES were determined using a Perkin Elmer Elan DRC–ICP–MS. Samples were introduced using a peristaltic pump at 1.0 mL per minute in conjunction with the auto sampler. Analysis was performed using an external calibration procedure, and internal standards were included to correct for matrix effects and instrumental drift correction [24,25]. Procedural blanks were analyzed to check for any contribution from the reagents.

### 3. Results and discussion

Upon sectioning the thermally treated samples, a layer of oxidized tin was observed at the tin/crucible interface, with oxidation increasing over greater exposure time. This was an unintended consequence due to the high porosity (23%) of the YSZ crucibles. The samples exposed for 2 h (W1 and P1) displayed the least amount of oxide formation, located only at the tin/YSZ interface. In addition to air leaking into the crucibles, tin also escaped through the YSZ crucibles in three of the samples (P3, W2, and W3), observed as tin mixed with sand outside the YSZ crucible in the bottom of the outer alumina crucible. The two Wyodak samples treated for 24 and 96 h (W2 and W3) were almost completely oxidized, and a considerable amount of tin leaked out, so these

**Table 2**  
Contents of each crucible.

Reductant source	Pittsburgh Seam coal (54% fixed C)	Wyodak Seam coal (48% fixed C)
Mixture weights	Sn = 1250 g SnO <sub>2</sub> = 125 g Coal = 18.28 g (100% stoich.) Cr = 33.9 mg Mo = 5.1 mg V = 9.6 mg CaO = 0.80 g	Sn = 1250 g SnO <sub>2</sub> = 125 g Coal = 23.99 g (115% stoich.) Cr = 33.1 mg Mo = 3.6 mg V = 7.8 mg CaO = 0.05 g
2 h	P1 (YSZ disk)	W1 (YSZ disk)
24 h	P2 (YSZ disk)	W2 (YSZ disk)
96 h	P3 (YSZ disk & strip)	W3 (YSZ disk & strip)



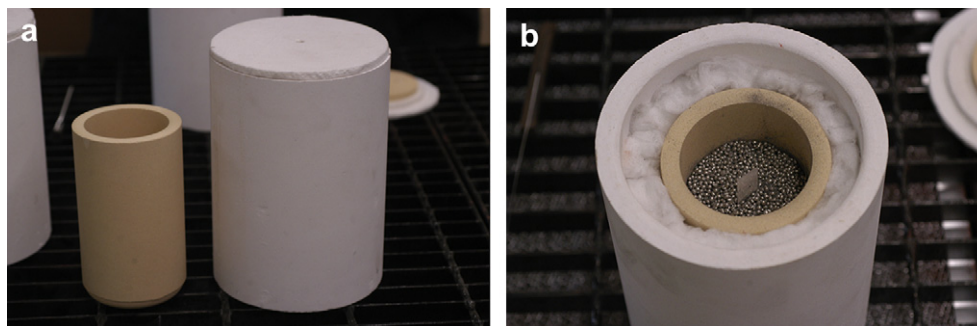


Fig. 2. (a) Crucibles before loading (YSZ on left, alumina on right), and (b) crucibles after loading (space between packed with sand).

samples were not analyzed. The two Wyodak samples being more oxidized than the Pitt Seam samples is believed due not to differences between the two coals, rather as the result of small variations in crucible porosity that allowed more air infiltration to oxidize the tin. The Pitt Seam sample exposed for 24 h (P2) was somewhat oxidized, with the oxide penetration about 0.5 cm in from the YSZ interface, but no tin had leaked out. The Pitt Seam sample treated for 96 h (P3) was heavily oxidized, but no tin had leaked out. The three Pitt Seam samples and W1 were polished for optical, SEM, and TEM characterization. A photo of these polished sections is shown in Fig. 3. The samples include a section of the tin/tin oxide along with the attached crucible so that the full interface could be characterized.

The locations of the YSZ disks and strip are shown in the figure. In P1 the YSZ disk floated to the top of the tin during the test, in W1 the disk stayed on the bottom of the crucible, in P2 it lifted up slightly off the bottom, and in P3 the strip remained vertical near the middle of the tin. A distinct tin oxide and slag layer formed on top of the ingots. The ingots contained voids, mainly between the tops of the ingots and the tin oxide/slag layer and the sides of ingots between the tin and the crucible wall, so an epoxy impregnation

technique was used where the tops and sides of the samples were infiltrated with epoxy before cutting and polishing in order to keep the sample intact for characterization. The following is a summary of the data obtained using SEM and TEM with EDS, and ICP analyses for each sample pictured in Fig. 3.

### 3.1. Sample P1 (Pitt Seam coal, 2 h)

The Pitt Seam sample held at temperature for 2 h (P1) contained a tin oxide layer at the tin/crucible interface, but the oxide layer did not penetrate far into the tin ingot. Critical interfaces within the sample are examined and include: crucible/tin; slag/tin; crucible/slag; and YSZ/tin. Fig. 4 shows an image taken from sample P1 at the tin/YSZ crucible interface along with the corresponding quantitative EDS results. A large gap is observed at this interface and Sn, C, Al, Si, and S are detected within the tin phase. The gap at the interface is most likely due to tin contraction and separation during cool-down and has been filled with epoxy during post-processing to maintain sample integrity. Porous tin oxide was also detected on both sides of the gap on the YSZ and the tin. Its formation on the interface suggests that the tin oxidized after being exposed to the air leaking through the crucible, and the material is not likely the original tin oxide powder. Tin sulfide particles, as shown in Fig. 4(b) and (c), were typically found in thin plate-like structures 10–50  $\mu\text{m}$  long in proximity to the tin oxide formations. The SnS melting temperature is 882  $^{\circ}\text{C}$ , therefore the structures were likely formed during sample cool-down, and the state of the sulfur at 1000  $^{\circ}\text{C}$  was not examined.

The P1 sample was also examined at the tin/slag interface, and as at the crucible/tin interface, instances of SnS attachment to tin oxide or slag particles were detected. SnS near this interface was also observed freely in the tin, but always in proximity to the oxide and slag-containing regions, and sometimes attached to them. Fig. 5 depicts a slag region in the P1 sample, which was found near the top of the tin ingot due to density effects, as expected. The main components of the slag are oxides of Al, Si, and Ca with smaller amounts of expected coal-derived slag formers including Na, K, Fe, and Ti. A small amount of V (0.13 at%), which was one of the spiking elements, was also measured in a slag particle in Spectrum 5.  $\text{SnO}_2$  was also found both attached to and in proximity to the slag particles, and carbon was observed in the slag particles in Spectrums 3 and 5. The most likely source of carbon in this case is from unreacted coal, since this region did not contain any pores or voids that could have been filled in with epoxy before the sample was sectioned and polished.

Detailed examination of the slag/tin interface of sample P1 was conducted by TEM to determine the slag constituency and to examine the interfacial features. Reactions between Sn and slag were also identified, and hundred nanometer-sized crystals of slag material were found adjacent to the tin and tin oxide nanograins

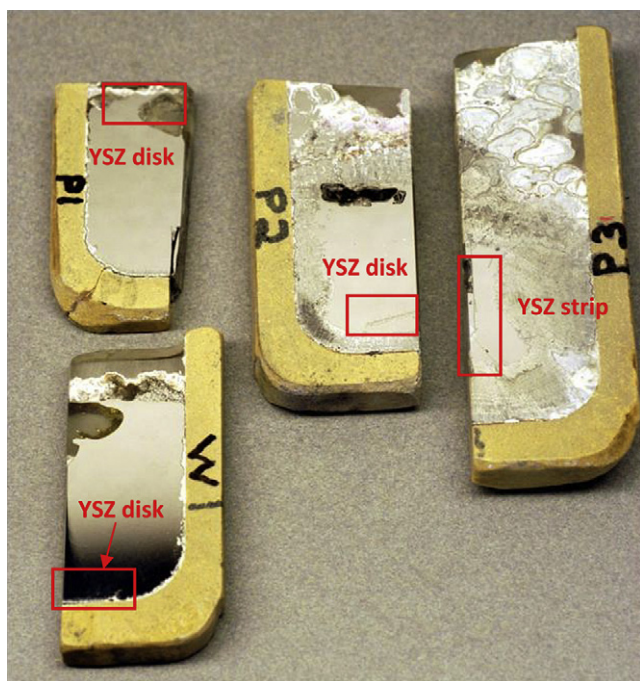


Fig. 3. Polished sections removed from crucibles that include a section of the tin/tin oxide ingot with the attached YSZ crucible. The locations of the YSZ disks and strip are also shown by the boxes.

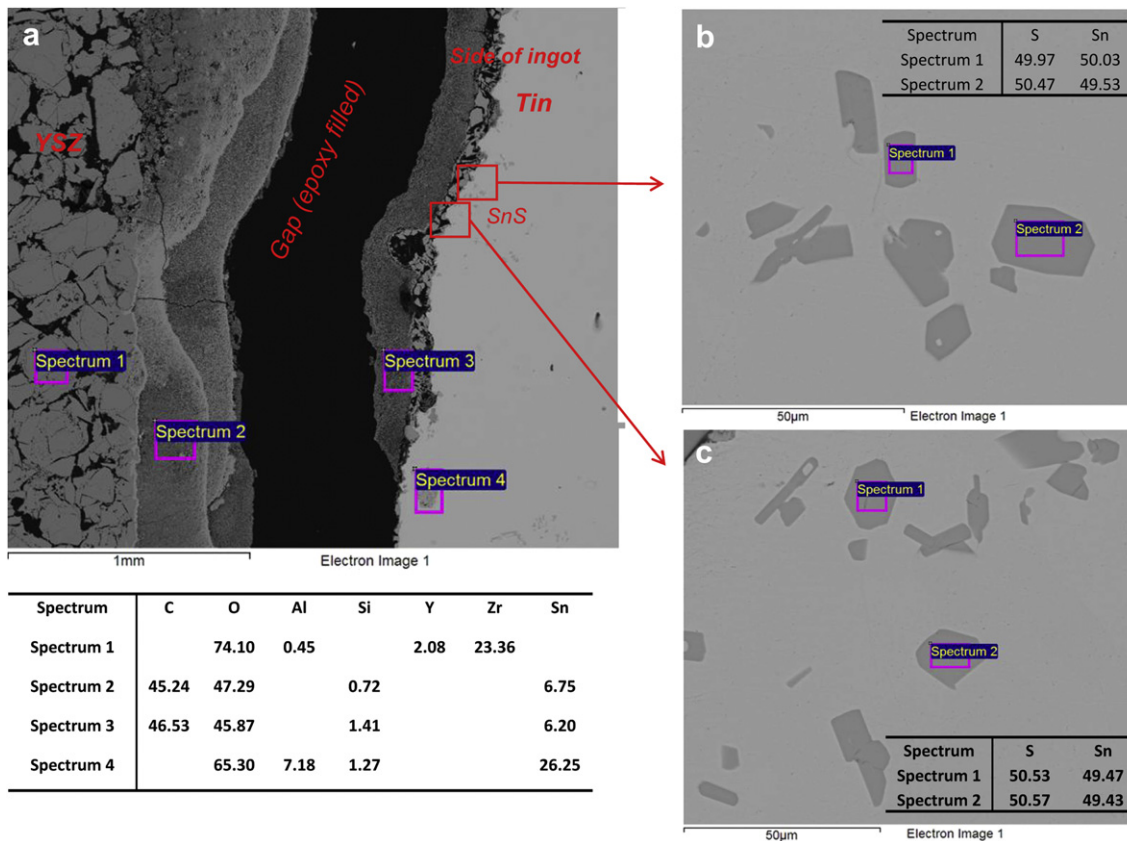


Fig. 4. SEM characterization with quantitative EDS results (at%) of the 2 h Pitt Seam sample (P1). (a) Side of the tin ingot adjacent to crucible wall with epoxy-filled gap between. (b) and (c) Zoomed-in regions containing SnS formations in the tin.

consisting of Sn–Si–Ca–Al–O. Both the electron diffraction pattern and the high-resolution TEM show that the Sn forms a solid solution in the Si–Ca–Al phase, and that no additional phases exist in the Sn–Si–Ca–Al–O phase. TEM examination was also completed

at the interface between the imbedded YSZ disk and the bulk tin. The framed region of sample P1 in Fig. 3 depicts the image location taken at the top of the YSZ disk that rose to the top of the tin during the test. TEM analysis with EDS revealed the presence of a tin oxide reaction layer on the YSZ, as shown in Fig. 6, although the Sn/O ratio appears to more closely correspond to tin monoxide. The electron diffraction from Sn [001] direction and YSZ [011] direction is shown in the insets of Fig. 6. The YSZ disk possesses a mixture of tetragonal YSZ and cubic YSZ, which are typical of YSZ electrolyte materials [26]. No other unusual structures or intergranular phases were detected in the sample.

ICP–AES/MS chemical analysis of the tin bulk from sample P1, shown in Table 3, was conducted to search for trace elements that may have been solubilized in the bulk tin. None of the three spiking elements (Cr, Mo, and V) were found in detectable amounts. Of the other contaminants of interest, only As and Mn were found, and only in quantities slightly exceeding the method detection limits (MDL). Arsenic was detected at 0.63 ppm (MDL = 0.4 ppm), and Mn at 0.16 ppm (MDL = 0.1 ppm). Al, Cu, Fe, and Pb were all found in significant concentrations, but similar to the concentrations existing in the as-received tin metal, implying that source impurities are culpable. Potassium was measured at over 5 ppm in the tin, and both coals contain a significant amount of K; therefore, the coal is the likely source. The potential impact of K on the fuel cell components is unknown.

3.2. Sample W1 (Wyodak coal, 2 h)

As with sample P1, the 2 h Wyodak sample (W1) was examined at critical internal interfaces and for bulk elemental composition. W1 also displayed an oxide layer at the tin/crucible interface

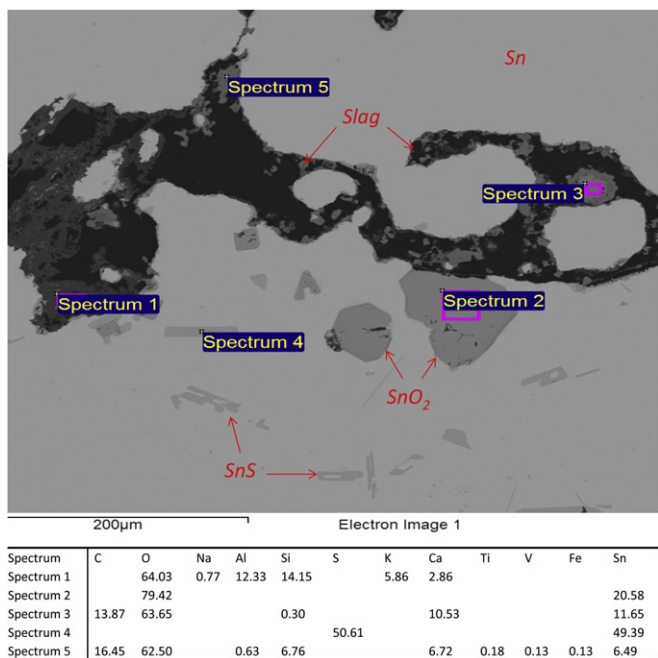
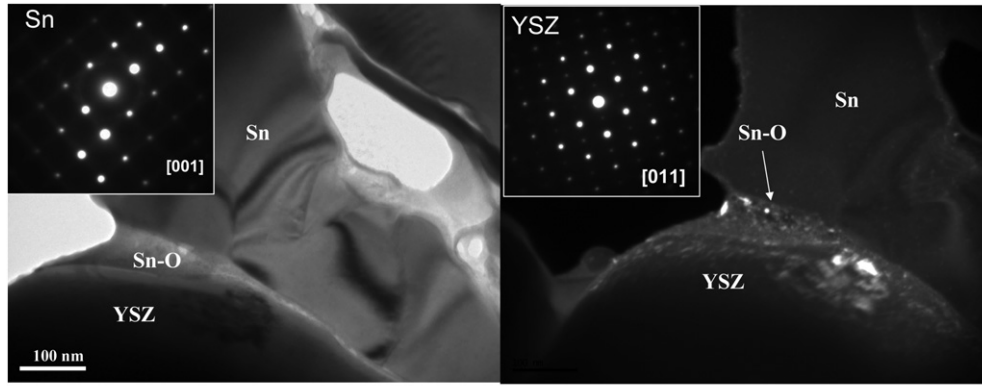


Fig. 5. SEM image of slag-containing area near top of tin in P1 sample with quantitative results from EDS (at%).



		C	N	O	Fe	Y	Zr	Sn
<b>Sn</b>	atom%	4.91		10.5		1.43	7.59	75.57
<b>Sn-O</b>	atom%		5.32	40.04		1.18	7.16	46.29
<b>YSZ</b>	atom%			30.09	0.15	10.87	58.62	0.29

Fig. 6. TEM image of polycrystalline Sn–O interface reaction layer that formed at the Sn–YSZ interface. Left: Bright field image; right: Dark field image.



similar in extent to P1. Unlike P1, the inserted YSZ disk remained in the bottom of the crucible during the test, but was somewhat broken up due to the weight of the charge above it. The crucible/tin and YSZ/tin interfaces can therefore be examined together, and Fig. 7 shows the SEM images and corresponding EDS analysis for both interfaces in W1. In the image in Fig. 7(a) the lower YSZ is the crucible, and the upper layer of YSZ is the disk that was inserted. A thin layer of tin exists between the YSZ layers. The dark spots in the YSZ crucible layer are voids, showing the considerable porosity of

the crucibles. A layer of tin oxide can be observed at the tin/crucible interface, and SnO<sub>2</sub> particles on the order of 30–60 μm were observed in the tin above the YSZ disk. EDS analysis of SnO<sub>2</sub> particles generally produces atomic quantification around 75 at% O and 25 at% Sn. The deviation from O:Sn stoichiometry of 2:1 is assumed to be an error in the result for oxygen, since EDS quantification is frequently inaccurate for light elements such as oxygen.

Some slag was found as hundred micron-sized particles near the YSZ disk surface, as shown in Fig. 7(b). The material is confirmed to

Table 3

ICP chemical analysis results for all samples along with both coals and the as-received tin oxide.

 = contaminant of interest  
 = spiking element

	mg/L (ppm)											
	Al	As	Ca	<del>Cr</del>	Cu	Fe	K	Mg	Mn	<del>Mo</del>	Na	Nb
SnO <sub>2</sub>	< 500	< 500	< 500	23	< 10	64	20	85	< 10	< 10	< 7	15
Pitt Seam coal	9120	7.0	1600	22	10	7655	1100	300	17	4	200	2.9
Wyodak coal	6161	1.4	12800	13	13	3376	100	1800	23	2.9	300	3
Tin metal	51	< 0.4	< 10	< 0.5	37	13.0	< 0.7	< 0.3	< 0.1	< 0.5	< 10	< 0.005
W1	61	0.61	< 5	< 0.5	20.2	16.4	12.01	< 0.3	0.15	< 0.5	< 10	< 0.005
P1	16	0.63	< 5	< 0.5	18.3	11.4	5.17	< 0.3	0.16	< 0.5	< 10	< 0.005
P2	78	< 0.4	< 5	< 0.5	22.0	24.6	5.99	< 0.3	0.13	< 0.5	< 10	< 0.005
P3	13	0.76	< 5	< 0.5	27.8	15.9	3.80	< 0.3	0.25	< 0.5	< 10	< 0.005

	Ni	P	Pb	S	Se	Si	Ta	U	<del>V</del>	W	Zn
SnO <sub>2</sub>	< 10		25	< 2	< 0.3	< 20	< DL	< 10	3	< 10	16
Pitt Seam coal	19	100	5.4	689	1.1	17800	0.16	0.69	30	4.0	25
Wyodak coal	14	300	2.7	4023	< 0.3	9400	0.16	0.58	16	8.9	14
Tin metal	7.0	< 15	129.0	< 0.3	< 2	< 2.5	< 0.005	< 0.005	< 2	< 0.005	< 0.3
W1	< 2	< 7	79.3	< 0.3	< 2	< 2.5	< 0.005	< 0.005	< 2	< 0.005	< 0.3
P1	< 2	< 7	76.0	< 0.3	< 2	< 2.5	< 0.005	< 0.005	< 2	< 0.005	< 0.3
P2	< 2	< 7	85.5	< 0.3	< 2	< 2.5	< 0.005	< 0.005	< 2	< 0.005	< 0.3
P3	< 2	< 7	129.2	< 0.3	< 2	< 2.5	< 0.005	< 0.005	< 2	< 0.005	< 0.3



be slag since oxides of Na, Al, Si, and K were clearly detected. The presence of slag on the YSZ disk was only observed in one other spot in this sample so was not considered to be widespread. As in P1, SnS was also observed in W1 and was usually present near tin oxide and slag formations near the top of the tin. The composition and shape of the microdomains of SnS in W1 are nearly identical to those observed in P1. The ICP results for bulk analysis of W1, as shown in Table 1 were similar to those for P1, with none of the three spiking elements detectable in quantities greater than the MDL, and only As and Mn having measurable amounts out of the contaminants of interest. No significant differences were seen between the two types of coals.

3.3. Sample P2 (Pitt Seam coal, 24 h)

The Pitt Seam sample thermally treated for 24 h (P2) displayed greater oxidation at the tin/crucible interface than P1, with the oxide penetrating into the tin approximately 0.5 cm. The inserted YSZ disk remained in the bottom of the crucible, but rose approximately 0.5 cm off the bottom and was tilted at an angle. The YSZ/tin interface was first examined, and Fig. 8 contains the SEM images and corresponding EDS results. Numerous particles were observed that contain tin and oxygen, and other smaller particles were determined to be SnS. The approximate Sn:O atomic ratio for SnO<sub>2</sub> was observed in most particles, which are located mainly above the YSZ disk in the tin, though in some cases they are attached. Fig. 8(b) magnifies a region above the YSZ disk and depicts the tin oxide particles around and on the YSZ. Fig. 8(c) depicts the bottom of the YSZ disk and shows a large SnO<sub>2</sub> particle directly attached to the YSZ, and numerous, sparsely detached particles of SnS. The size, shape, composition, and distribution of SnO<sub>2</sub> and SnS in this region are similar to those features observed in P1 and W1.

The SEM image in Fig. 9 contains a representative sample of the slag/tin interface in P2 taken near the upper regions of the ingot. The slag consists of at least two different phases, one containing more Sn (dark gray) and one containing more Al and Si (black). Both phases contain approximately 14–16 at% C, although accurate carbon quantification using EDS is difficult, as with oxygen. The C is most likely from unreacted coal, as there are no other major sources of carbon present in the system at that location. Fig. 9 also depicts

a large SnO<sub>2</sub> particle and a smaller SnS particle that appear to be attached to the slag. In more than one case, Cr particles encased in an oxidized shell were observed within the slag. None of the three spiking elements (Cr, Mo, and V) were found in the tin in P2 from the ICP analysis (Table 3). Of the contaminants of interest, only Mn was detected, although the result was only 0.13 ppm (MDL = 0.1 ppm).

3.4. Sample P3 (Pitt Seam coal, 96 h)

The Pitt Seam sample thermally treated for 96 h (P3) was heavily oxidized, with only a small amount of tin metal remaining in the middle. The YSZ strip that was inserted vertically remained in the middle of the tin, although it became slightly tilted. The YSZ/tin interfaces were examined, and the SEM images and EDS results show SnS particles in the tin proximal to and attached to the YSZ strip, similar to what is shown in Fig. 8 for sample P2.

P3 was also examined at the region near the top of the tin ingot where some slag species were evident, as shown in Fig. 10. Fig. 10(a) shows that the darker regions contain mostly oxides of the primary slag-forming metals, Al, Si, and Ca, along with smaller amounts of Fe and V. A significant amount of tin is also found within the slag particles. Carbon is also observed in the slag and is most likely unreacted carbon from the source coal. Fig. 10(b) shows additional slag particles surrounded by tin and interspersed with SnO<sub>2</sub> and SnS particles. Of the three spiking elements added to each sample (Cr, Mo, and V), Cr and V were observed in the slag, but none were found in the tin bulk by ICP analysis (Table 3). Molybdenum was not found in the tin by ICP or in the slag from EDS. None of the other contaminants of interest were located in the tin by ICP analysis.

3.5. Comparison and summary of results

Examination of the results obtained from all four samples reveals that similar features were observed at each of the interfaces and in the bulk. In general, the slag floated on top of the tin bath due to its lower density, although slag particles were also observed to have formed on the submerged YSZ in at least two cases. The effect of the CaO addition was not evident. This was likely due, at least in part, to the small scale of the tests, in which slag generation

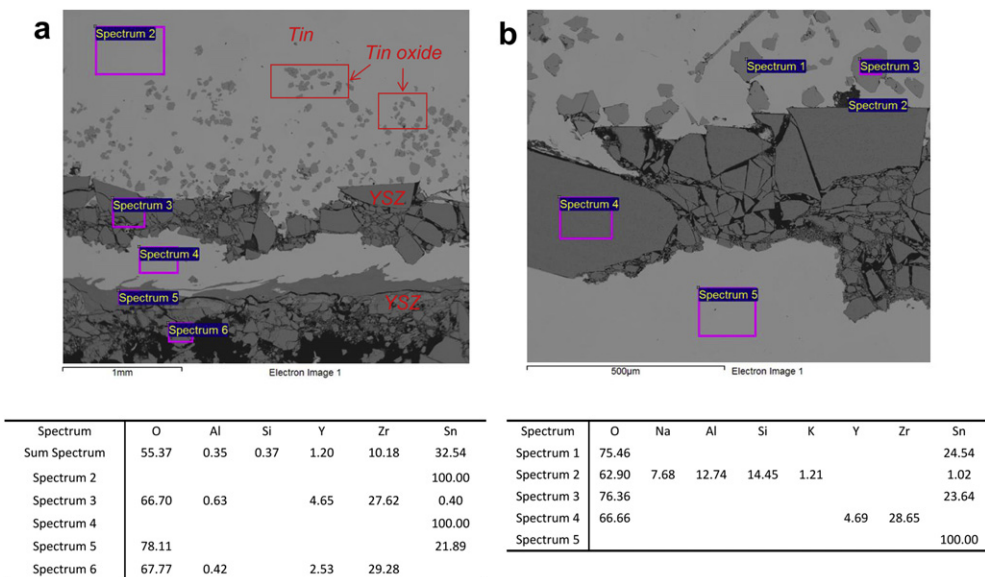
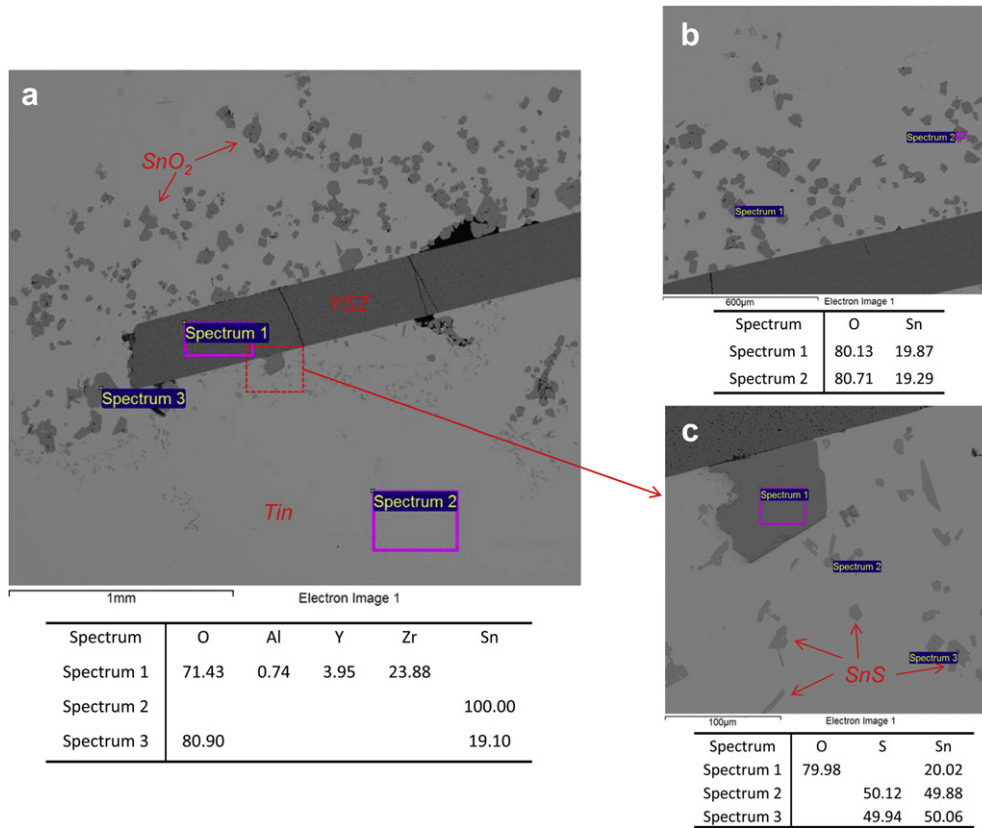
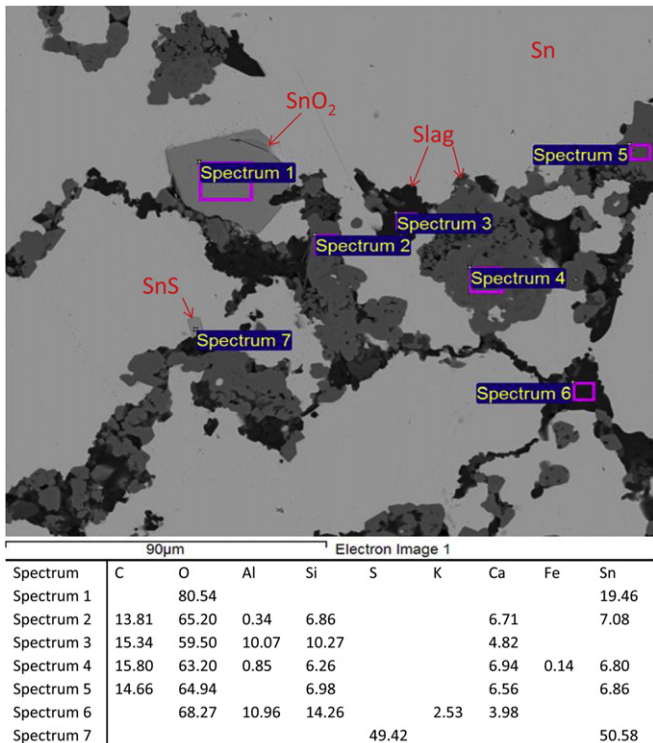


Fig. 7. SEM characterization of 2 h Wyodak sample (W1) showing YSZ disk in the bottom of the YSZ crucible. (a) SnO<sub>2</sub> particles exist both in the tin above the YSZ disk and attached to the YSZ. Image (b) is magnified to show a slag particle attached to a YSZ grain (Spectrum 2).



**Fig. 8.** SEM images with EDS results on 24 h Pitt Seam (P2). (a) View of the YSZ disk submerged in the tin in the bottom of the crucible. (b) Magnified region above the YSZ disk showing SnO<sub>2</sub> particles. (c) Magnified region of the bottom of the YSZ disk showing the SnO<sub>2</sub> particle attached to the disk and SnS particles.



**Fig. 9.** SEM image with EDS results for slag-containing region in top of tin in sample P2.

was too small to result in the formation of a slag layer that could be sampled effectively and the partitioning calculated quantitatively.

No significant differences were observed in a comparison of results between the two types of coals. The Wyodak coal contains higher levels of sulfur according to the chemical analysis of the as-received coals, as shown in Table 3, indicating about 4000 ppm of sulfur in the Wyodak and 700 ppm in the Pitt Seam coal. Absolute quantification of sulfur content in the samples is difficult as sulfur is not homogeneously located, but qualitative differences in the samples were not observed. One must note however that only one sample was analyzed from the Wyodak coal, thus making the comparison less certain. The only noted differences observed pertained to the oxide growth at the tin/crucible interface over time, which was related to oxygen infusion through the porous crucibles and is not fundamentally important to LMA SOFC operation. It would be beneficial to re-run the experiments for the sake of reproducibility and in order to confirm any potential differences in behavior between the coals, but owing to the consistency among the cells tested the existing data set is considered sufficiently reliable.

The observed SnO<sub>2</sub> growth on YSZ must be considered as a possible impediment in cell operation. SEM analysis clearly shows SnO<sub>2</sub> particles of 30–100 µm attached directly to YSZ surfaces at the YSZ/tin interfaces. TEM analysis also provided evidence of the existence of a nanoscale tin oxide reaction layer forming between YSZ and tin. These observations support results obtained by Jayakumar et al. [19], which indicated a decrease in the cell performance over time of a LTA SOFC. Degradation was attributed to the formation of a tin oxide layer on the electrolyte that limited the transport of oxygen ions from the electrolyte into the tin anode. The operating temperature and current density of a LTA SOFC system



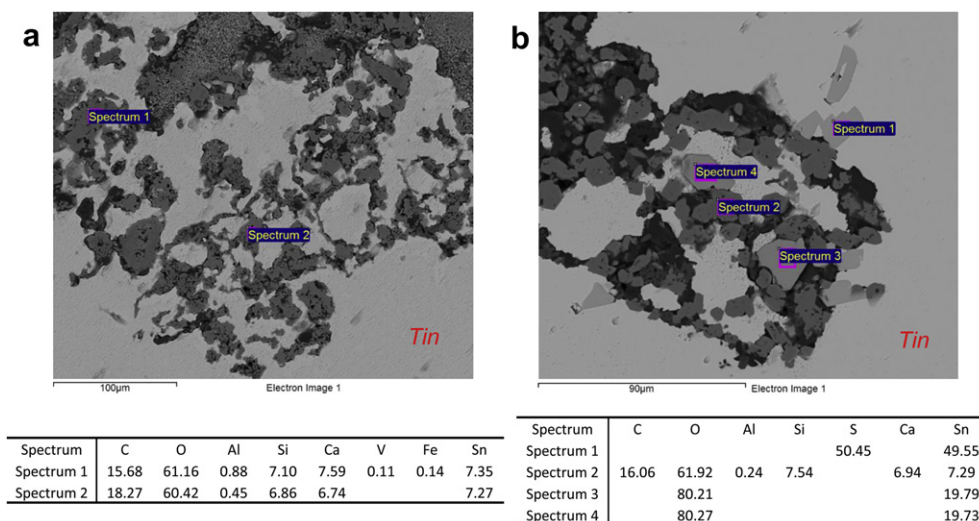


**Fig. 10.** SEM images with EDS results for 96 h Pitt Seam sample (P3) showing regions of slag near the top of the tin region. (a) Particles consist of oxides of Al, Si and Ca along with small amounts of V and Fe, and a considerable amount of Sn. (b) Particles of SnO<sub>2</sub> and SnS mixed in with the slag particles.

must thus be controlled in a way to prevent the formation of solid SnO<sub>2</sub>, keeping any oxygen present dissolved in the liquid tin phase.

A second striking feature observed in all samples was the formation of microdomains of SnS. The SnS phases were identified in both slag/tin interfaces and proximal to YSZ/tin interfaces, with some SnS directly attached to YSZ. The microdomains indicate that S is solubilized by Sn during operation and likely precipitates heterogeneously at different tin interfaces during cell cooling. With the given relative amounts of tin and coal used in these experiments at 1000 °C, a secondary liquid SnS is not expected to form, as the reported solubility of S in Sn at that temperature is around 8 at% [27]. This solubility limit is higher than the sulfur content of the coal itself. Sulfur was previously hypothesized to oxidize and exhaust as a volatile gas, essentially behaving as a fuel. The observation of SnS in all samples, including the four day exposure, combined with the known presence of excess oxygen in the system diminishes this possibility.

The third major observation is of the presence of Sn pockets within the slag/tin interface regions. Microdomains of Sn at the slag/tin interface imply that some metallic tin may be encapsulated. If operations required removal of the slag-forming ash component by skimming or filtering, a significant amount of tin could also be lost. Continuous tin addition would be required to make up for the loss, and a tin recovery process must be considered, adding to the complexity of the system.

The distribution of carbon was also examined within the system. Carbon was observed in the slag formations at roughly the same magnitudes in all samples, indicating time-independent retention of unreacted coal. A similar feature was observed in preliminary tests, when samples were held at 1000 °C for 1 h, therefore, the present samples were thermally treated for a longer duration to facilitate more complete combustion of the coal. Given the observation of unreacted coal particles in the slag regions, one concludes that in the present experimental setup, 100% coal reaction efficiency is not possible.

Various other elements were observed by ICP and SEM/EDS, though no evidence of degradative processes was observed, and no abnormal structures were detected at the critical interfaces. Arsenic was detected and could be a concern, although the levels are low (<1 ppm). Significant amounts of Pb were also found in each tin sample (100 ppm range), and although Pb readily alloys with Sn, it is not considered a contaminant of interest. Copper and Fe were

measured in all tin samples at amounts of roughly 20 ppm. Aluminum was measured in amounts that varied from 13 to 61 ppm. The likely source of these metals is from the as-received tin metal since the analysis of the as-received tin showed levels of Al, Cu, Fe, and Pb that were close to the measured amounts found in the tin from each sample after exposure. Although these elements are obviously present, the impact (if any) to performance is not yet known.

### 3.6. Thermodynamic modeling

To more fully explore the interaction of sulfur and tin and to consider how to remove dissolved sulfur from molten tin, the thermodynamic software package FactSage™ 6.1 [28,29] was used to find the thermodynamic equilibrium between Sn, S, O, H, and C. For these calculations, the FACT, FACT53, and FTmisc (for dealing with soluble species in tin) databases were used for thermodynamic properties of possible constituents.

When looking at just Sn, S, and excess O at 1000 °C, solid SnO<sub>2</sub> will always form (once the oxygen solubility limit in liquid tin is exceeded) before SO<sub>2</sub> gas due to their relative Gibbs energy of formations. Sulfur will first dissolve in tin, meaning the cell can operate in the presence of sulfur, but once the solubility limit of sulfur is exceeded, liquid SnS will begin to form (since the melting point of SnS is 882 °C). The boiling point of SnS is 1230 °C, giving it an appreciable vapor pressure, although with only Sn, S, and O, FactSage does not predict the formation of SnS vapor at 1000 °C. As the sulfur content in coal can vary between 0.4 and 4 wt%, even if only a fraction of this sulfur is accessible to the tin (as some of the sulfur in coal is in the form of other sulfides, some of which are more stable than SnS), depending on the thickness of the tin layer, a significant amount of sulfur could build up in the tin within hours to a few days of operation. This would mean the tin would then have to be purified to prevent the formation of SnS (either as a solid precipitate at lower temperatures or as a secondary liquid phase at higher temperatures).

However, when the tin, oxygen, and sulfur are put in a reducing atmosphere (with either carbon or hydrogen), SnS vapor will form, an important fact for sulfur removal. Adding hydrogen to the mixture drives the formation of water, hydrogen sulfide (H<sub>2</sub>S) gas, and SnS vapor. At 800 °C, below the melting point of SnS, the ratio of H<sub>2</sub>S to SnS vapor is greater than six, meaning the sulfur can be

removed from the tin as H<sub>2</sub>S, in hydrogen excess, with only a little loss of tin as SnS vapor. By 1000 °C, the H<sub>2</sub>S:SnS vapor ratio drops to around 0.75, so most of the sulfur being removed from the molten tin would be taking some tin with it in the vapor phase. If the formation of water is suppressed, the formation of H<sub>2</sub>S and SnS will increase, but only marginally shift the H<sub>2</sub>S:SnS ratio in favor of H<sub>2</sub>S. Using coal in abundance (mostly carbon, with a small amount of available hydrogen), would form H<sub>2</sub>, H<sub>2</sub>O, CO, H<sub>2</sub>S, SnS vapor, as well as some CH<sub>4</sub> in the gas phase.

Thus, the presence of hydrogen in the system may diminish the solubilized sulfur content by producing volatile H<sub>2</sub>S and SnS vapor, but the claim is made from a thermodynamic argument, and more experiments would need to be performed to test that claim under different steady state conditions. In this case, it is suggested hydrogen could be used in small amounts as a gas clean-up method. Knowledge of the final disposition of sulfur in LMA SOFC is ultimately important due to the well documented negative effects of sulfur on YSZ [9,11,12,21–23].

#### 4. Conclusion

Mixtures of tin, coal, and spike contaminants were thermally treated and analyzed to examine thermochemical reaction modes potentially leading to degradation in liquid tin anode solid oxide fuel cells. SEM/EDS characterization of four samples identified three principal phenomena that could be detrimental to the operation of a LTA SOFC fueled directly by coal. First, SnO<sub>2</sub> was observed to form on and near tin/YSZ interfaces, which may impede oxygen exchange reactions in an operating LTA SOFC. Second, SnS was observed to form within the tin, mainly near the SnO<sub>2</sub> and slag particles and the YSZ. This indicates that sulfur accumulation is a potential concern in these cells, if a suitable means of sulfur removal cannot be found. Third, tin metal, tin oxide, and carbon were all found to be intermixed with the slag, which may complicate the slag removal and tin recovery processes.

Of the three spiking elements added to the samples (Cr, Mo, and V) only Cr and V were detected in the slag using EDS and none of the three were detected in the tin metal in the ICP chemical analysis. No Mo was detected by EDS in the tin or slag components, or from the ICP results on the tin. Of the other contaminants of interest, only As and Mn were detected above analytical limits, though both elements were present at <1 ppm and only marginally higher than the method detection limits. Elements such as Pb, Cu, Fe, and Al were detected in the bulk tin at levels consistent with the source material impurities.

The principal goal of this work was to evaluate contaminate partitioning due to thermochemical drivers in a system containing the primary materials of a LMA SOFC. An important continuation of the work would be to then take such information and propose methods by which the problems can be mitigated. Design of comprehensive LTA SOFC systems directly operating on solid fuels will require continued research to assess the impact of the observed degradations on operation. Mitigation of operational issues associated with the identified problems can likely be addressed by engineering and design improvements. The role of anode composition must be explored to determine whether the impact of oxide and sulfide formation may be diminished. Research related to oxygen transport, including evaluation of solubility and diffusion in the liquid metal anode must be continued, and contaminant impacts reassessed for each potential alloy and electrolyte system.

#### Acknowledgments

This technical effort was performed in support of the ongoing research at NETL under the RES contract DE-FE0004000. The

authors wish to thank Paul Danielson for his work in preparing and polishing samples, Jinesh Jain for conducting the chemical analysis at NETL facilities in Pittsburgh, Phillip Gansor and Ed Sabolsky at West Virginia University for providing the YSZ disks and strips tested, and the LMA SOFC Regional University Alliance (RUA) team for their useful feedback.

This report was prepared as an account of work sponsored by an agency of the United States Government. Neither the United States Government nor any agency thereof, nor any of their employees, makes any warranty, express or implied, or assumes any legal liability or responsibility for the accuracy, completeness, or usefulness of any information, apparatus, product, or process disclosed, or represents that its use would not infringe privately owned rights. Reference herein to any specific commercial product, process, or service by trade name, trademark, manufacturer, or otherwise does not necessarily constitute or imply its endorsement, recommendation, or favoring by the United States Government or any agency thereof. The views and opinions of authors expressed herein do not necessarily state or reflect those of the United States Government or any agency thereof.

#### References

- [1] U.S. Department of Energy, Fuel Cell Handbook, seventh ed. EG&G Technical Services, Inc., Nov. 2004, under contract #DE-AM26-99FT40575.
- [2] U.S. Department of Energy, Energy Information Administration, Annual Energy Outlook 2011 DOE/EIA-0383 (April 2011), [www.eia.gov/forecasts/aeo/](http://www.eia.gov/forecasts/aeo/).
- [3] U.S. Department of Energy, Current and future technologies for gasification-based power generation, In: A Pathway Study Focused on Carbon Capture Advanced Power Systems R&D Using Bituminous Coal, vol. 2 (Nov. 2010) DOE/NETL-2009/1389.
- [4] D. Cao, Y. Sun, G. Wang, J. Power Sources 167 (2007) 250–257.
- [5] X. Li, Z. Zhu, R. de Marco, J. Bradley, A. Dicks, J. Power Sources 195 (2010) 4051–4058.
- [6] Lawrence Livermore National Laboratory, Science & Technology Review, Turning Carbon Directly into Electricity, June 2001.
- [7] S. Nürnberg, R. Bubar, P. Desclaux, B. Franke, M. Rzepka, U. Stimming, Energy Environ. Sci. 3 (2010) 150–153.
- [8] T.M. Gür, M. Homel, A.V. Virkar, J. Power Sources 195 (2010) 1085–1090.
- [9] R.J. Gorte, H. Kim, J.M. Vohs, J. Power Sources 106 (2002) 10–15.
- [10] Z.F. Zhou, C. Gallo, M.B. Pague, H. Schobert, S.N. Lvov, J. Power Sources 133 (2004) 181–187.
- [11] J. Bao, G.N. Krishnan, P. Jayaweera, K.-H. Lau, A. Sanjurjo, J. Power Sources 193 (2009) 617–624.
- [12] Z. Cheng, S. Zha, M. Liu, J. Power Sources 172 (2007) 688–693.
- [13] C. Sun, U. Stimming, J. Power Sources 171 (2007) 247–260.
- [14] Z.F. Zhou, R. Kumar, S.T. Thakur, L.R. Rudnick, H. Schobert, S.N. Lvov, J. Power Sources 171 (2007) 856–860.
- [15] H. Abernathy, R. Gemmen, K. Gerdes, M. Koslowski, T. Tao, J. Power Sources 196 (2011) 4564–4572.
- [16] W.A.G. McPhee, M. Boucher, J. Stuart, R.S. Parnas, M. Koslowski, T. Tao, B.A. White, Energy Fuels 23 (2009) 5036–5041.
- [17] Tao, et al., Electrochemical device and methods for energy conversion, Filed: Nov. 25th, 2009, Issued: May 17th, 2011, U.S. Patent: 7943271.
- [18] M. LaBarbera, M. Fedkin, S. Lvov, Electrochem. Soc. Trans. 35 (1) (2011) 2725.
- [19] A. Jayakumar, S. Lee, A. Hornés, J.M. Vohs, R.J. Gorte, J. Electrochem. Soc. 157 (3) (2010) B365–B369.
- [20] T. Tao, CellTech Power, Novel Fuel Cells for Coal Based Systems, SECA Conference, Pittsburgh, July 2010, Report #DOE/NETL-2010/1430, [www.netl.doe.gov/publications/proceedings/10/seca/index.html](http://www.netl.doe.gov/publications/proceedings/10/seca/index.html).
- [21] K. Sasaki, et al., J. Electrochem. Soc. 153 (11) (2006) A2023–A2029.
- [22] J.N. Kuhn, N. Lakshminarayanan, U.S. Ozkan, J. Mol. Catal. A: Chem. 282 (2008) 9–21.
- [23] L. Zhang, S.-P. Jiang, H.-Q. He, X. Chen, J. Ma, X.-C. Song, Int. J. Hydrogen Energy 35 (2010) 12359–12368.
- [24] J.C. Jain, C.R. Neal, J.M. Hanchar, Geostandards Newslett. 25 (2001) 229–237.
- [25] M.A. Schneegurt, J.C. Jain, J.A. Menicucco Jr., S. Brown, D.F. Garafalo, M. Quallick, C.R. Neal, C.F. Kulpa Jr., Environ. Sci. Technol. 35 (2001) 3786–3791.
- [26] Y. Chen, S. Chen, H. Finklea, X. Song, G. Hackett, K. Gerdes, Solid State Ionics 204–205 (2011) 87–90.
- [27] R.C. Sharma, Y.A. Chang, J. Phase Equilib. Diffusion 7 (1986) 269–273.
- [28] C.W. Bale, P. Chartrand, S.A. Degterov, G. Eriksson, K. Hack, R. Ben Mahfoud, J. Melancon, A.D. Pelton, S. Petersen, Calphad 26 (2002) 189–228.
- [29] C.W. Bale, E. Bélisle, P. Chartrand, S.A. Degterov, G. Eriksson, K. Hack, I.H. Jung, Y.B. Kang, J. Melancon, A.D. Pelton, C. Robelin, S. Petersen, Calphad 33 (2009) 295–311.